Optimization of Ethanol Flow Rate for Improved Catalytic Activity of Ni Particles to Synthesize MWCNTs Using a CVD Reactor

Muhammad Mansoor*, Muhammad Shahid, Amir Habib

School of Chemical and Materials Engineering, National University of Sciences and Technology – NUST, Islamabad, Pakistan

During synthesis of MWCNTs using CVD, role of carbonaceous material and catalyst, besides other process parameters, has considerable influence on the structure and yield of pristine nanotubes. In present study, different flow rates (i.e. 10, 25, 40 and 55 sccm) of precursor ethanol were used for the synthesis of MWCNTs at 750 °C in a CVD reactor, where nickel particles were supported on quartz as catalyst. Further, these nanotubes were characterized using XRD, SEM, TGA and Raman spectroscopy to investigate the effect of ethanol flow rate on the catalytic activity of nickel for optimum production of MWCNTs. It was observed that at different ethanol flow rates, variations in synthesis products (i.e. CNTs, amorphous carbon and carbon nanoparticles) were associated with catalytic activity. Maximum catalytic activity of nickel particles was attained by optimizing ethanol flow rate (at 25 sccm). At the optimum flow rate a maximum purity of MWCNTs (>83%) was attained along with other relevant structures i.e. amorphous carbon <1.5% and SWCNT <10% balancing with retained catalytic particles. Any increase from the optimum limit caused not only defects within the CNTs' structure but also increased the impurities which were correlated with the reduction in activity of the nickel particles due to the saturation of active sites.

Keywords: *multiwall carbon nanotubes, catalytic activity, catalytic CVD, ethanol flow rate, TGA, Raman spectroscopy*

1. Introduction

CNTs are allotropes of carbon. A single-walled carbon nanotube (SWCNT) is a one-atom thick sheet of graphite, called graphene, rolled-up into a seamless cylinder with diameter in the order of a nanometer, which results in a nanostructure where the aspect ratio may exceeds 1,000,000. In multi-walled carbon nanotubes (MWCNTs) a single sheet of graphite is rolled-in around itself, resembling a scroll of a newspaper. The interlayer spacing in MWCNT is close to the distance between graphene layers in graphite; approximately 3.3 Å[1,2]. CNTs have novel properties that make them potentially useful in many applications in nanotechnology, electronics, optics, composites and other fields of materials science. They exhibit extraordinary strength and unique electrical properties, and are efficient conductors of heat[3-5].

There are several approaches to produce CNTs in sizeable quantities, including arc discharge[6], laser ablation[7], and chemical vapor deposition (CVD)[8]. Most of these processes take place in vacuum or with process gases. CVD growth of CNTs can take place in vacuum or at partial pressure.

During CVD, a substrate is prepared with a layer of metal catalyst particles, most commonly nickel, cobalt, iron, or a combination. The metallic nanoparticles can also be produced by other ways, including reduction of oxides or oxides solid solutions. The diameters of CNTs that are to be grown are related to the size of the catalytic particles[8]. This can be controlled by patterned (or masked) deposition of the catalyst, annealing, or by plasma etching of a catalyst layer. The substrate is heated to approximately 900 °C. To initiate the growth of CNTs, two gases are blended into the reactor: a process gas (such as ammonia, nitrogen, hydrogen, etc.) and a carbon-containing gas (such as acetylene, ethylene, methane, etc.). Nanotubes grow at the sites of the metal catalyst; the carbon-containing gas is broken apart at the surface of the catalyst particle, and the carbon is transported to the edges of the particle, where it forms the nanotubes. The mechanism is still under discussion however, the catalyst particles can stay at the tips of the growing nanotube during the growth process, or remain at the nanotube base, depending on the adhesion between the catalyst particle and the substrate[9].

Of the various means for CNTs synthesis, CVD shows the most promising industrial scale deposition in terms of its economics. There are additional advantages to the CVD synthesis of CNTs: unlike the other methods, CVD is capable of growing nanotubes directly on a desired substrate, whereas other processes demand an additional step for collection of CNTs. The growth sites are controllable by careful deposition of the catalyst. Moreover, CVD also supports to grow vertically aligned carbon nanotubes (VACNTs) using various carbon precursors with the liberty of supported or floating catalysts. One of the popular

*e-mail: muhammadmansoor@scme.nust.edu.pk

methods to synthesize VACNTs is co-evaporation technique, where catalyst and carbon precursor are mixed. The mixture is then evaporated and passed through the CVD reactor having inert atmosphere, where synthesis and deposition of CNTs occurs. Main advantage of the process is "long active growth period" for the synthesis of CNTs due to continuous supply of catalyst along with carbon precursor. Resultant CNT products are usually a thick mat of vertically aligned CNTs[10-13].

Maruyama et al.[14] are the pioneer researchers who reported synthesis of SWCNT using ethanol. They prepared dual metallic catalyst supported on zeolite by sonication-assisted mixing of iron acetate and cobalt acetate in ethanol with Y-type zeolite powder. In a CVD reactor the catalyst mixture was placed and ethanol vapors were passed from an ethanol reservoir (at room temperature) using a vacuum pump. The SWCNTs were synthesized at 700-800 °C.

Extending the Maruyama's work, Kouravelou et al.[15] exhibited their work on dynamic study of CNT growth using ethanol. They used iron oxide particles supported on alumina and studied the effect of catalytic particle loadings on the carbon yield. A mixture of ethanol, methanol, hydrogen and helium was used for CNT synthesis. The CNTs produced were of multi-walled type.

Mendoza et al.[16] introduced a variation in Maruyama's approach by passing hydrogen gas through an ethanol bubbler and synthesizing MWCNTs at 700 °C and 900 °C on quartz supported catalyst (iron nitrate). They increased the length of MWCNTs using a process temperature of 700 °C, by inhibiting generation of amorphous carbon caused by -OH radicals.

In 2009, Maruyama and his team again reported their work with an approach to reactivate the catalyst by introducing acetylene in ethanol assisted CNT growth. This time they used Co/Mo mixture as catalyst at a process temperature of 800 °C and ethanol/acetylene as precursor. They observed a 10-fold increase in the growth of SWCNTs by catalytic reactivation[17].

Another research group, Ren Yan et al.[18] demonstrated synthesis of free standing SWCNTs film using ferrocene and ethanol. They employed two furnaces for this purpose; one for the evaporation of ferrocene/ethanol mixture at 100 °C and the other for pyrolysis of ethanol and synthesis of the CNTs. By varying the flow rate of ethanol they observed variations in the CNTs diameter, however, they did not show explicit data about the ethanol flow rates.

Recently, Jaime et al.[19] has mentioned the effect of ethanol precursor on the synthesis of MWCNTs using perovskite-type oxide $LaNiO_3$ as catalyst. They found that the catalyst is quite efficient for ethanol decomposition producing $3.5g_{cnt}.(g_{cat}.h)^{-1}$ at 700 °C and 50ml.min^{-1} of ethanol in He (50 % - v/v).

As mentioned above, the previous researchers[14-19] had shown their work on alcohol assisted SWCNT growth by CVD but the effect of ethanol flow rate for the synthesis of MWCNTs associating catalytic activity of nickel particles during CVD was ignored.

In the present study, MWCNTs were grown on quartz substrates in a CVD reactor where ethanol was used as a precursor with nitrogen and hydrogen as inert carrier and reducing medium, respectively. The flow rate of nitrogen gas was used to introduce various concentrations of ethanol during the synthesis of MWCNTs and subsequently, the effect of various ethanol flow rates on the deposited CNTs was studied with respect to the catalytic activity of the nickel particles. The characterization was carried out using X-ray diffractometer (XRD), scanning electron microscope (SEM), thermal gravimetric analysis (TGA) and Raman spectroscopy.

2. Experimental

2.1. *Description of CVD process*

A horizontal tube furnace was used with nitrogen as a carrier gas and as dilution medium for the injection of ethanol whereas hydrogen was used as a reducer gas. A quartz substrate was coated with nickel nitrate solution as catalyst. A hydrogen treatment was carried out for nickel nitrate reduction prior to the CNT synthesis. Subsequently, a controlled flow of ethanol, hydrogen and nitrogen was introduced at 750 °C for CNT growth. Ethanol bubbler was kept at 45 °C during bubbling process. Typically, a process of 20 minutes of CNT growth was used to deposit CNTs at a flow rate of 10 sccm of hydrogen and 10, 25, 40 and 55 sccm of ethanol vapors via nitrogen bubbler. A schematic view of the CVD reactor is shown in Figure 1. The CNTs batches synthesized at 10, 25, 40 and 55 sccm of ethanol vapors were named as A-CNTs, B-CNTs, C-CNTs and D-CNTs, respectively.

2.2. *Synthesis sequence*

The synthesis of CNTs was carried out in five stages:
- **Coating:** A homogeneous thin film of nickel nitrate solution (50mmol/l) was coated on the quartz substrates using a spin coater. Thickness of the deposited film was assured to be same in each case by using fixed coating parameters (i.e. solution concentration, feed quantity, feed rate and spinning speeds). Subsequently, the coated substrates were dried in an oven at 65 °C for 2 hours. After drying, the coated substrates were placed in the CVD reactor.
- **Decomposition:** Nickel nitrate thermally decomposes at 350 °C to nickel mono-oxide according to the Equation 1[20]:

$$2Ni\,(NO_3)_2 \rightarrow 2NiO + 4NO_2 + O_2 \qquad (1)$$
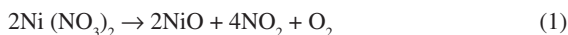
Therefore, the coated substrates were heated to 350 °C at the rate of 5 °C/min. and held at this temperature for 30 minutes to attain a complete decomposition to nickel mono-oxide. The slower heating rate was desired to favor a gradual decomposition of the catalyst; or it might cause splashes resulting in heterogeneous distribution of the catalyst on the substrate.
- **Reduction:** The reactor temperature was raised to 450 °C and hydrogen gas (10 sccm) along with nitrogen gas (25 sccm) were introduced in the reactor for 10 minutes to reduce the nickel oxide into nickel nano particles.
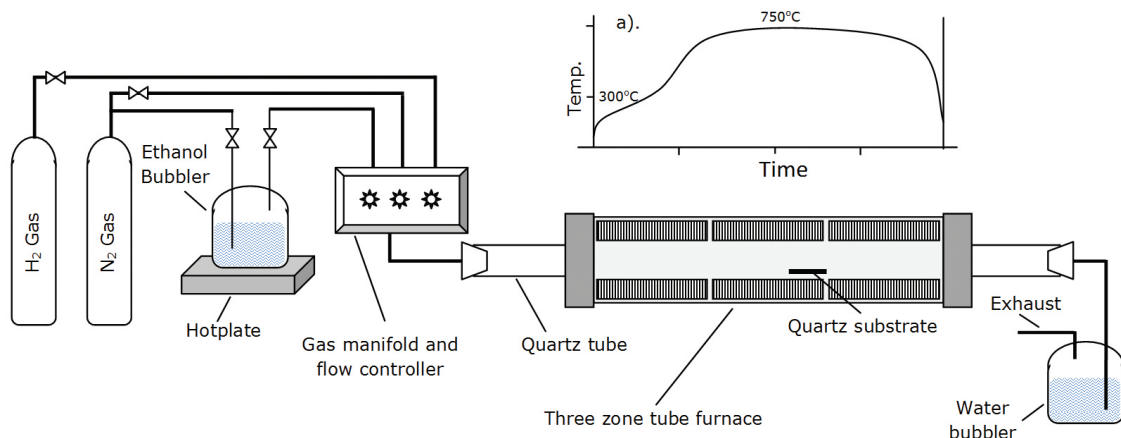
2014; 17(3)

Optimization of Ethanol Flow Rate for Improved Catalytic Activity
of Ni Particles to Synthesize MWCNTs Using a CVD Reactor

741

Figure 1. Schematic of the CVD apparatus; a) is the inset of the reactor's temperature profile during CNT synthesis.

- **Synthesis:** Finally, the reactor temperature was raised to 750 °C at a heating rate of 25 °C/min. A relatively fast heating rate was helpful to avoid coarsening of nickel nano particles due to high temperature and longer time period. At reaction temperature, hydrogen gas was maintained at the same flow rate whereas nitrogen gas was bubbled through ethanol; various ethanol flow rates were used to synthesize CNTs. This process was continued for 20 minutes.
- **CNTs removal:** The processed substrates were washed in 0.4M HCl at 45 °C to remove the CNTs deposit. The removed deposits were washed and filtered with de-ionized water and heated in oven at 65 °C for 1 hour before desiccation. Various stages of the synthesis are graphically presented in Figure 2.
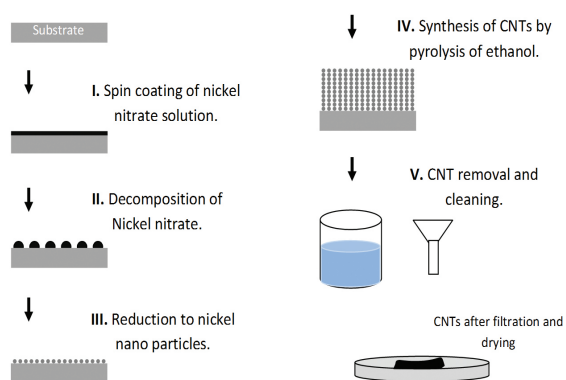

Figure 2. Various stages for the synthesis of CNTs.

3. Results and Discussion

3.1. *X-ray diffraction*

Powder samples of various CNT batches were subjected to XRD analysis using a Cu Kα radiation source and a scan rate of $0.05°$ s^{-1} from $18°$-$75°$ (2θ). The resultant XRD scans are given in Figure 3. The scans are superimposed on each other with a vertical off-set of 1000 CPS.

Three peaks of different intensities observed in each scan i.e. $26.5°$, $45°$ and $52°$ are shown in the figure. The major peak which can be attributed to hexagonal graphite occurred around $26.5°$ and it represents (002) planes of CNTs[21,22]. Other two minor peaks represent the nickel catalytic particles [PDF card No: 040850]. The intensity of the $26.5°$ peak reflects the quantity and the crystallinity of carbon phase in the form of CNTs[23]. The scans indicated that at flow rate of 10 standard cubic centimeters per minute (sccm) i.e. for A-CNTs, amount of amorphous carbon was relatively high which rapidly diminished as the flow rate ascended to 25 sccm (B-CNTs). However, it again increased with increasing flow rates i.e. 40 and 55 sccm in the case of C- and D- CNTs, respectively. Other two peaks i.e. $45°$ and $52°$ represent variation in the amounts of nickel particles with their intensities, while the peak broadenings depict their nanocrystalline size.
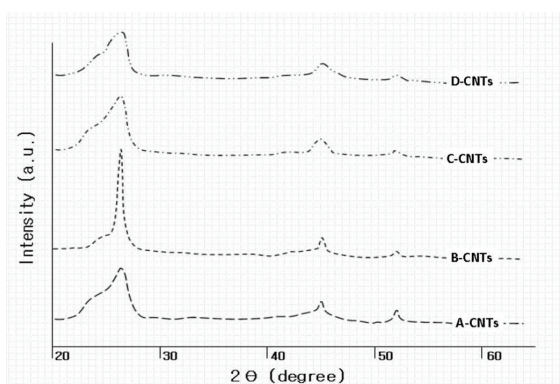

Figure 3. Superimposed XRD scans of various CNT batches, peaks at $26.5°$ represent graphite (002), while peaks at $45°$ and $52°$ represent nickel catalytic particles entrapped in the CNTs.

3.2. *Scanning electron microscopy*

For SEM studies, loose powder of the CNTs was directly sprinkled on the adhesive carbon tape supported by an aluminum stub. Further the sprinkled CNTs were gently pressed with a glass slide to ensure the CNTs were properly fixed on the carbon tape. The micrographs are shown in

Figure 4, which were exposed in secondary electron imaging mode at 20KV.

In A-CNT specimen the CNTs were irregular in shape, structurally inconsistent and heterogeneous (Figure 4a). The fine CNTs were stemming out from the coarse CNTs. Trapped catalytic nickel particles were present at the ends and body of the CNTs; presumably the fine CNTs were nucleated from the trapped nickel particles causing more heterogeneous growth pattern during synthesis.

In B-CNT specimen, regular and uniform strands of CNTs were observed (Figure 4b). Amorphous carbon was

seen in isolated regions in minute quantity. In C-CNT and D-CNT specimens, an increasing trend of structural heterogeneity, randomness and amorphous carbon was observed. The maximum heterogeneity was observed in D-CNT specimen (Figure 4c and d). Additionally, transmission electron microscopy (TEM) of B-CNT specimen was also carried out. A dilute suspension of the specimen in ethanol was prepared by sonication and dropped on a holey carbon coated grid. The specimen was studied in bright field mode at 200KV. A uniform spread of diameter (10 nm ± 2nm) was observed in the nanotubes of B-CNT
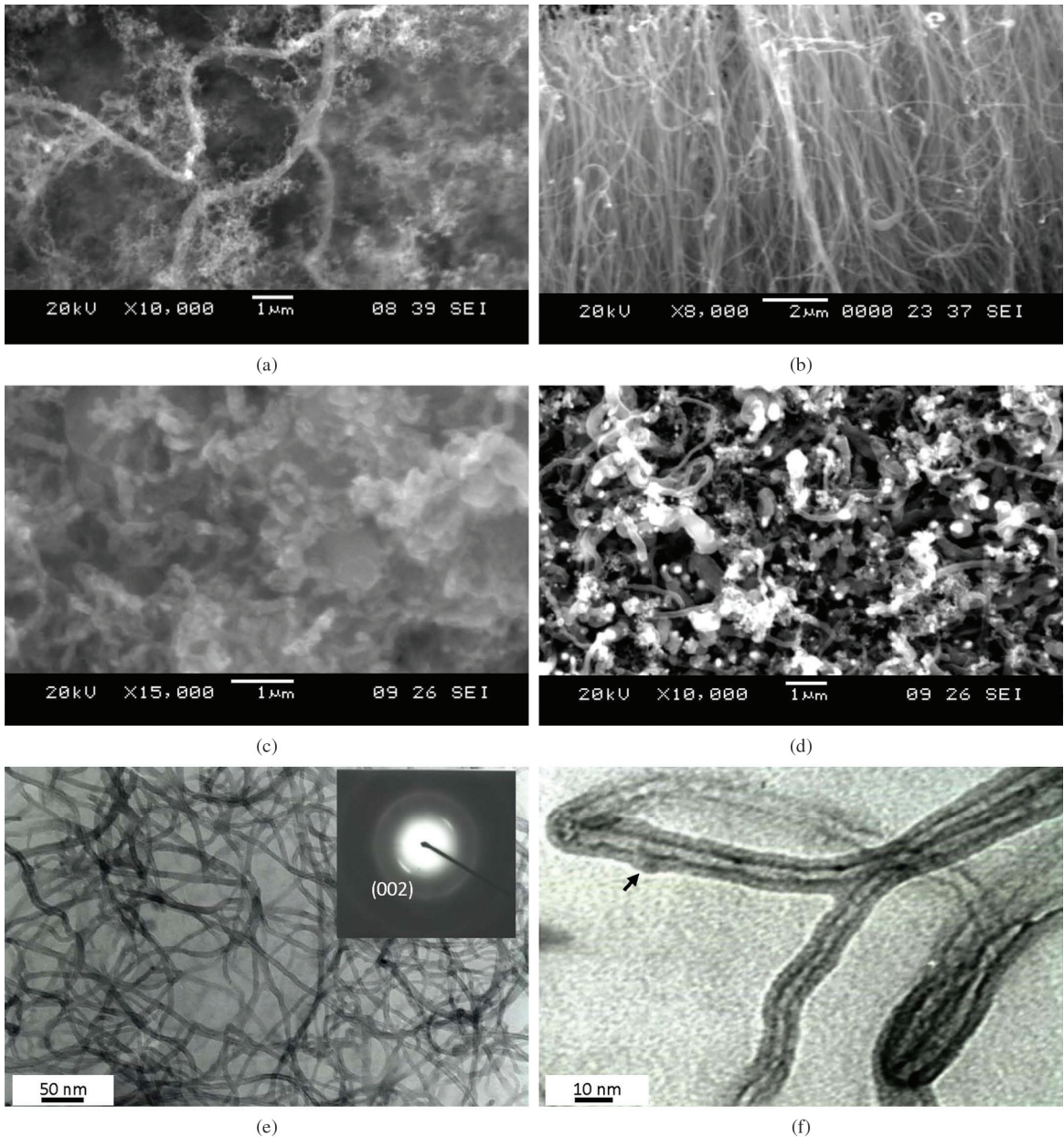

Figure 4. SEM micrographs of the CNTs from various batches i.e. a) A-CNT, b) B-CNT, c) C-CNT and d) D-CNT. Figures e) and f) are TEM images of B-CNT batch, showing long MWCNTs. Inset is characteristic diffraction pattern of MWCNTs showing (002) reflections. Amorphous carbon is evident on the walls of the nanotubes (arrow).

2014; 17(3)

Optimization of Ethanol Flow Rate for Improved Catalytic Activity
of Ni Particles to Synthesize MWCNTs Using a CVD Reactor

743

specimen. At higher magnification, amorphous carbon was seen on the outer walls of the nanotubes (Figure 4e and f). The inset in Figure 4e is diffraction pattern of the nanotubes showing their multi-walled nature with (002) reflections.

The comportment of CNT synthesis during the process could be attributed to the variation of ethanol flow rates as well as to the catalytic activity. Since the other process parameters were kept constant in all formulations equal amount of catalyst (ca.) were available for reaction in various ethanol concentrations, which helped in cracking and subsequent growth of carbon molecules in to CNTs. Increasing flow rate of ethanol from 10 sccm to 25 sccm resulted in better structural control and uniformity in growth of the CNTs. The CNTs were more regular in shape, uniform in structure and less contaminated by amorphous carbon. A further increase in ethanol flow rate caused structural damage to the synthesized CNTs; this could be attributed to sluggish activity of catalyst particles, which was unable to decompose increased carbon contents into MWCNTs. This hypothesis was further supported by TGA results.

3.3. *Thermogravimetric analysis*

For TGA studies, 10mg of the CNTs from each formulation were heated to 900 °C in air using a Netzsch STA 409C system. A heating rate of 10 °C/min and a constant flow of air were maintained throughout the heating cycle. The TGA plots along with the analyses of the various CNTs specimens are shown in Figures 5a-d, which depict fractional thermal stability of CNTs in terms of variation in mass during heating in air. Each plot consists of three curves, TGA, DTGA and Lorentzian fitting of DTGA, represented by solid line, dash-dot line and dash line, respectively.

The TG curves demonstrated oxidation start temperatures of various specimens at temperatures in the range of 310-360 °C, indicating the oxidation temperature of amorphous carbon present; the variation in the oxidation start temperatures suggests various levels of defects in the specimens[24]. A similar type of work is also reported by other researchers as well[25,26]. After initial drop in mass, the curves overlapped during the later stages and were difficult to interpret directly. Therefore, their differential curves (DTGA) were plotted to elucidate the change in mass with increasing temperatures. The DTGA curves showed mass changes at documented temperature ranges for different phases present in the samples (315-355 °C for amorphous carbon, 429-486 °C for SWCNTs, 582-602 °C for MWCNTs and 670 °C for carbon nano-particles (CNPs))[27].

The quantitative analysis of each phase corresponds to its area under the peak, and was executed by means of Lorentzian fitting of the DTGA curves. Lorentzian curve fitting resulted in up to four fractional steps marked as step-I, step-II, step-III and step-IV, representing amorphous carbon, SWCNTs, MWCNTs and CNP, respectively[27,28]. In A-CNTs, a heterogeneous multiphase deposit was observed since maximum fraction was represented by amorphous carbon and SWCNTs. However, small quantities of MWCNTs and CNPs were also present in the specimen. In B-CNTs, more than 80% of the specimen fraction was occupied by MWCNTs besides diminishing fractions of amorphous carbon and SWCNT. In C-CNTs and D-CNTs specimens, increasing tendencies of amorphous carbon along with decreasing fractions of MWCNTs were observed.

To find activity of the catalyst, a modified approach was adopted, where the amount of MWCNTs synthesized
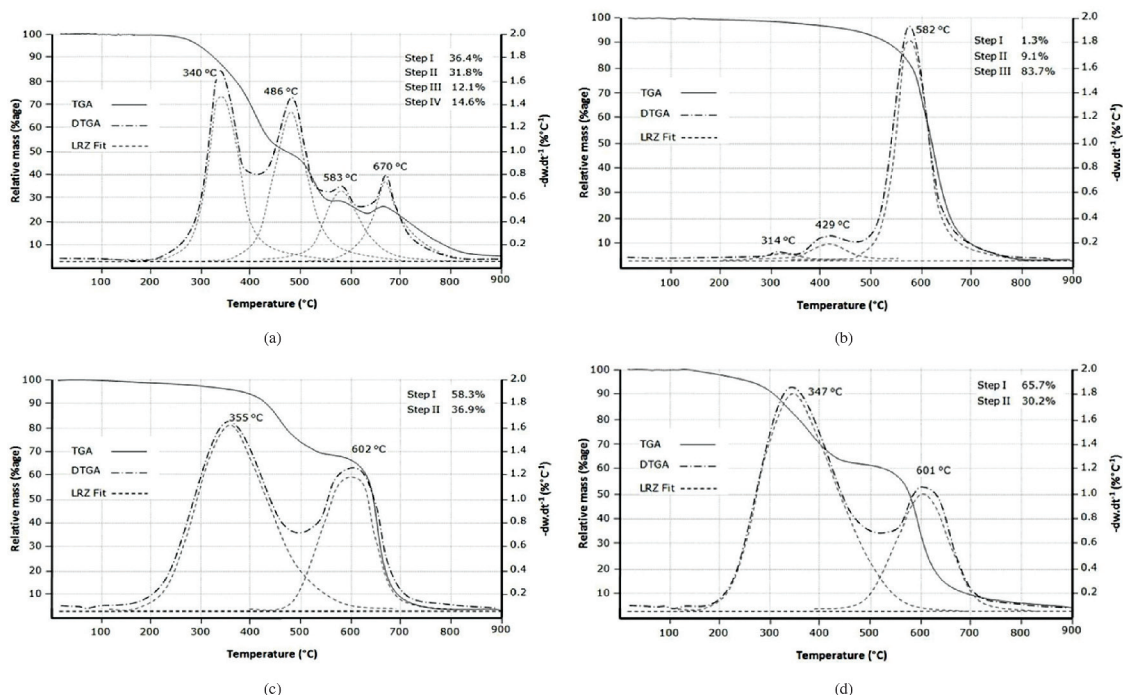

Figure 5. TGA curves of various CNTs specimens i.e. a) A-CNTs, b) B-CNTs, c) C-CNTs and d) D-CNTs, showing worked graphs of DTGA and Lorentzian fitting.

was assumed to be directly related with activity of catalytic particles (i.e. nickel). The catalytic activity (H_{ct}) was calculated using following formula[29]:

$$H_{ct}(\%) = 100(M_p - M_r)/M_r \qquad (2)$$

where M_r was the weight of the catalyst retained during TGA, which was actually consumed to decompose ethanol and Mp was the weight of the resulted CVD product (here the product is specifically MWCNTs). To control the skewness of the calculated H_{ct} values, the catalytic activity was plotted on log scale. The results obtained after TGA analyses are shown in Table 1 and graphically represented in Figure 6.

Table 1 indicates that maximum purity of synthesized MWCNTs was achieved with an ethanol flow rate of 25-30 sccm, whereas minimum littering by other phases was also occurred. Any further increase in the flow rate resulted in increased levels of other phases. Moreover, a varying quantity of retained catalytic particles were also observed with ethanol flow rate, which suggests that with increasing flow rate a saturation in the activity of nickel particles occurred, as indicated in Table 1. The low activity of the nickel particles resulted in copious generation of unwanted phases especially amorphous carbon.

In Figure 6, calculated catalytic activity of nickel particles at different ethanol flow rates is plotted. It was observed that catalytic activity of Nickel particles increased rapidly with ethanol flow rate and attained its optimum values at 25-30 sccm, afterwards it decreased rapidly and became steady around 50-55 sccm of ethanol flow rate.

3.4. *Raman spectroscopy*

Raman analysis was carried out using a Raman Renishaw spectrometer operating with a wavelength of 785 nm. The specimens were manually compressed between two glass slides in order to improve density to get measurable spectrum. Each specimen was scanned in the Raman shift range of 100-3000 cm⁻¹. A superimposed montage of the curves is shown in Figure 7, where three critical Raman shift ranges for D, G and G' bands have been collected. The D-band represents defects in MWCNTs including sp^3 bonded carbonaceous impurities and broken sp^2 bonds. G-band emerges owing to graphitic nature of the specimen exhibiting crystallinity and the atomic structure. Whereas G'-band appears due to the long-range ordering of the structure and is developed from two-phonon second order scattering process resulting in generation of an inelastic phonon[30].

Instead of using intensity ratios of D- and G- bands to qualitatively assess purity levels of MWCNTs specimens[25], the mathematical formulae proposed by DiLeo et al.[31] were used. They used a set of reference samples with known percentage of MWCNTs and selective synthesized by-products. Changes in the characteristic Raman peak ratios were measured as a function of MWCNTs contents. They also proposed following three equations to calculate ratios of D-, G-, and G'- bands in order to evaluate purity of the respective MWCNTs specimens:

$$D/G_{ratio} = 0.96 - 0.0066X \qquad (3)$$

$$G'/G_{ratio} = 0.33 + 0.0045X \qquad (4)$$

Table 1. The results obtained by TGA analyses of various synthesized CNTs specimens.

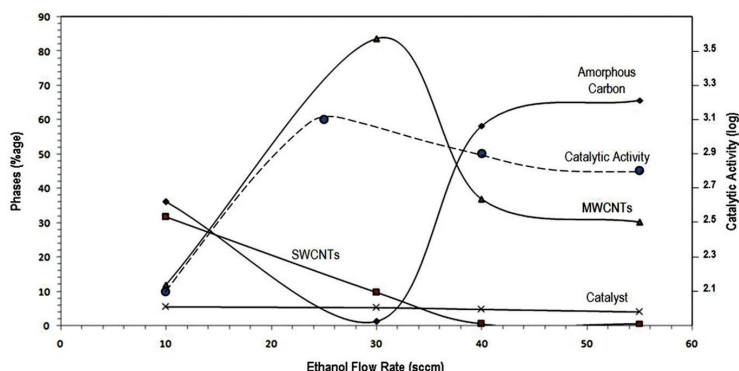| Sample	Ethanol Flow Rate (sccm)	Amorphous Carbon (%age)	SWCNTs (%age)	MWCNTs (%age)	Carbon Nano Particles (%age)	Retained Catalyst (%age)	Catalyst Activity (log scale values)
A-CNTs	10	36.4	31.8	12.1	14.6	5.1	2.1
B-CNTs	25	1.3	9.1	83.7	-	5.9	3.1
C-CNTs	40	58.3	-	36.9	-	4.8	2.9
D-CNTs	55	65.7	-	30.2	-	4.1	2.8

Figure 6. Graphs of the variation in different phases along with ethanol flow rates (solid lines), changes in catalytic activity with ethanol flow rates (dashed line).
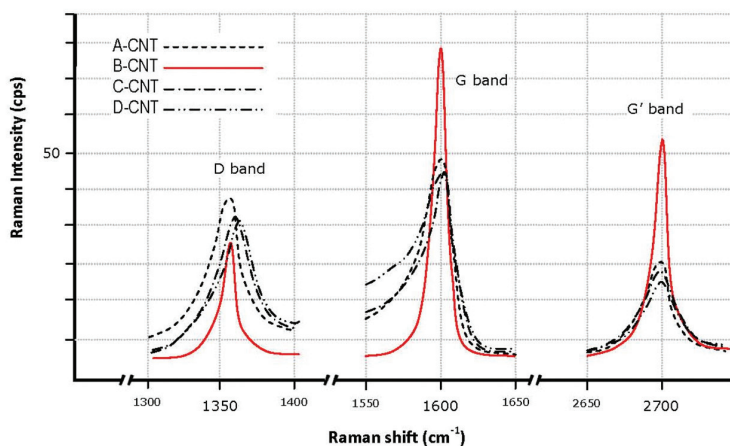
2014; 17(3)

Optimization of Ethanol Flow Rate for Improved Catalytic Activity
of Ni Particles to Synthesize MWCNTs Using a CVD Reactor

745

Figure 7. A superimposed montage of the Raman curves of the specimens encompassing selection of the critical Raman shift ranges for MWCNTs.

Table 2. Measured intensities of various Raman spectrums along with calculated purity (in terms of MWCNTs) by the curve fitting formulae.

Specimen ID	D-band	G-band	G'-band	MWCNT present in various specimens (%age)			
				D/G Curve fit	G'/G curve fit	G'/D curve fit	Average Purity
A-CNTs	42	58	30	35.7	41.6	39.7	39.0
B-CNTs	35	89	62	85.8	81.5	83.0	83.4
C-CNTs	41	56	27	34.5	33.8	35.9	34.7
D-CNTs	42	55	24	29.7	27.7	29.1	28.8

$$G'/D_{ratio} = 0.31 * \exp(0.21X) \qquad (5)$$

where, 'X' is the percentage of MWCNTs. By taking the intensities of the characteristic peaks from individual Raman spectrum, the amount of MWCNTs present in each specimen was calculated using above mentioned equations. The results are shown in Table 2. It could be seen that the results obtained by Raman spectrometry are quite comparable with TGA with only exception of A-CNT specimen, which probably arises due to the presence of SWCNTs and CNPs as the above mentioned equations were derived for the specimens containing MWCNTs and synthesis products other than SWCNTs.

4. Conclusions

Ethanol assisted synthesis of MWCNTs was realized in a CVD reactor successfully. Maximum yield of MWCNTs (>83%) was attained by optimizing ethanol flow rate and catalytic activity of nickel particles. An ethanol flow rate of 20-30 sccm with other described operational parameters, proved to be optimum for efficient synthesis of MWCNTs as evident by various characterization techniques, however, nickel particles rendered maximum activity. A variation in ethanol flow rate other than the optimum value (20-30 sccm) caused formation of excessive amorphous carbon and synthesis products along with MWCNTs, resulting in decrease in efficiency of overall process. The structural homogeneity of the CNTs is attributed to the nickel catalytic activity.

References

1. Dresselhaus MS, Dresselhaus G and Saito R. Carbon nanotubes: Physics of carbon nanotubes. *Carbon*. 1996; 33:27-35.

2. Dresselhaus MS. *Science of Fullerences and Carbon Nanotubes*. San Diago: Academic Press; 1996. p. 153-160.

3. Harris PJ. *Carbon Nanotubes and Related Structures*. Cambridge: Cambridge Press; 1999. p. 84-93. PMid:10378632. http://dx.doi.org/10.1017/CBO9780511605819

4. Xie S, Li W, Pan Z, Chang B and Sun L. Mechanical and physical properties of carbon nanotubes. *Journal of Physics and Chemical Society*. 2000; 61:1153-1158. http://dx.doi.org/10.1016/S0022-3697(99)00376-5

5. Ajayan PM and Zhou OZ. Applications of carbon nanotubes. *Carbon Nanotubes: Topics in Applied Physics*. 2001; 80: 391-425. http://dx.doi.org/10.1007/3-540-39947-X_14

6. Iijima S. Helical microtubules of graphitic carbon. *Nature*. 1991; 354:56-58. http://dx.doi.org/10.1038/354056a0

7. Ting G. Catalytic growth of single-walled nanotubes by laser vaporization. *Chemistry Physics Letters*. 1995; 243:49-54. http://dx.doi.org/10.1016/0009-2614(95)00825-O

8. Eftekhari A, Jafarkhani P and Moztarzadeh F. High-yield synthesis of carbon nanotubes using a water-soluble catalyst support in catalytic chemical vapor deposition. *Carbon*. 2006; 44:1343-1352. http://dx.doi.org/10.1016/j.carbon.2005.12.006

9. José-Yacamán M. Catalytic growth of carbon microtubules with fullerene structure. *Applied Physics Letters*. 1993; 62:657-664. http://dx.doi.org/10.1063/1.108857

10. Singh C, Shaffer MSP, Koziol KKK, Kinloch IA and Windle AH. Towards the production of large-scale aligned carbon nanotubes. *Chemical Physics Letters.* 2003; 372:860-865. http://dx.doi.org/10.1016/S0009-2614(03)00531-1

11. Kumar M and Ando Y. A simple method of producing aligned carbon nanotubes from an unconventional precursor - Camphor. *Chemical Physics Letters.* 2003; 374:521-526. http://dx.doi.org/10.1016/S0009-2614(03)00742-5

12. Musso S, Fanchini G and Tagliaferro A. Growth of vertically aligned carbon nanotubes by CVD by evaporation of carbon precursors. *Diamond & Related Materials.* 2005; 14:784-789. http://dx.doi.org/10.1016/j.diamond.2004.12.030

13. Dassios KG, Musso S and Galiotis C. Compressive behavior of MWCNT/epoxy composite mats. *Composites Science and Technology.* 2012; 72:1027-1033. http://dx.doi.org/10.1016/j.compscitech.2012.03.016

14. Maruyama S, Kojima R, Miyauchi Y, Chiashi S and Kohno M. Low-temperature synthesis of high-purity single-walled carbon nanotubes from alcohol. *Chemical Physics Letters.* 2002; 360:229-234. http://dx.doi.org/10.1016/S0009-2614(02)00838-2

15. Kouravelou KB and Sotirchos SV. Dynamic study of carbon nanotubes by chemical vapor deposition of alcohol- Review. *Advanced Materials Science.* 2005; 10:243-248.

16. Mendoza D, Santiago P and Reyes Pérez E. Carbon nanotubes produced from hexane and ethanol. *Revista Mexicana De F'IsicaCarta*. 2006; 52:1-5.

17. Xiang R, Einarsson E, Okawa J, Miyauchi Y and Maruyama S. Acetylene-accelerated alcohol catalytic chemical vapor deposition growth of vertically aligned single-walled carbon nanotubes. *Journal of Physical Chemistry C.* 2009; 113(18):7511-7515. http://dx.doi.org/10.1021/jp810454f

18. Yan R, Wen-Jun M, Qing-Sheng Z, Jin-Zhu L, Hai-Bo D and Wei-Ya Z. Carbon nanotube synthesized from ethanol and its oxidation behavior in air. *Chinese Physics B.* 2012; 21(9):0981031-6.

19. Jaime G, Germán SG, Carlos D, Rafael M, Joël B, Catherine B et al. Production Of Carbon Nanotubes and Hydrogen by Catalytic Ethanol Decomposition. *Dyna, year 80*. 2013; 178:78-85.

20. Brockner W, Ehrhardt C and Gjikaj M. Thermal decomposition of nickel nitrate hexahydrate, $Ni(NO_3)_2 \cdot 6H_2O$, in comparison to $Co(NO_3)_2 \cdot 6H_2O$ and $Ca(NO_3)_2 \cdot 4H_2O$. *Thermochimica Acta*. 2007; 456:64-71. http://dx.doi.org/10.1016/j.tca.2007.01.031

21. Zhao LP and Gao L. Coating of multi walled carbon nanotubes with thick layers of tin (IV) oxide. *Carbon.* 2004; 42:1858-1867. http://dx.doi.org/10.1016/j.carbon.2004.02.013

22. Li YH, Wang HG, Cao AY, Zhao D, Zhang XF, Xu CL et al. Adsorption of florid from water by amorphous alumina supported on carbon nanotubes. *Chemistry Physics Letters*. 2001; 350:412-415. http://dx.doi.org/10.1016/S0009-2614(01)01351-3

23. Buang NA, Fadil F, Majid ZA and Shahir S. Characteristic of mild acid functionalized multiwalled carbon nanotubes towards high dispersion with low structural defects. *Digest Journal of Nanomaterials and Biostructures*. 2012; 7(1):33-39.

24. Scheibe B, Borowiak-Palen E and Kalenczuk RJ. Oxidation and reduction of multiwalled carbon nanotubes -preparation and characterization. *Materials Characterization*. 2010; 61:185-191. http://dx.doi.org/10.1016/j.matchar.2009.11.008

25. Shaffer MSP and Windle AH. Fabrication and Characterization of Carbon Nanotube/Poly(vinyl alcohol) composites. *Advance Materials*. 1999; 11:937-941. http://dx.doi.org/10.1002/(SICI)1521-4095(199908)11:11<937::AID-ADMA937>3.0.CO;2-9

26. Konstantinos G and Dassios CG. Polymer-nanotube interaction in MWCNT/ poly(vinyl alcohol) composite mats. *Carbon*. 2012; 50:4291-4301. http://dx.doi.org/10.1016/j.carbon.2012.04.042

27. Lehman JH, Terrones M, Mansfield E, Hurst KE and Meunier V. Evaluating the characteristics of multiwall carbon nanotubes. *Carbon*. 2011; 49:2581-2602. http://dx.doi.org/10.1016/j.carbon.2011.03.028

28. Shi Z, Lian Y, Liao FH, Zhou X, Gu Z and Zhang Y. Large scale synthesis of single-wall carbon nanotubes by arc-discharge method. *Journal of Physics and Chemistry of Solids*. 2000; 61:1031-1036. http://dx.doi.org/10.1016/S0022-3697(99)00358-3

29. Dung ND, Chuc NV, Tam NTT, Quang NH, Khoi PH and Minh PN. Carbon-nanotube growth over iron nanoparticles formed on $CaCO_3$ support by using hydrogen reduction. *Journal of the Korean Physical Society*. 2008; 52(5):1372-1377. http://dx.doi.org/10.3938/jkps.52.1372

30. Saito R, Grüneis A, Samsonidze GG, Brar VW, Dresselhaus G, Dresselhaus MS et al. Double resonance Raman spectroscopy of single-wall carbon nanotubes. New Journal of Physics. 2003; 5:157.1-15.

31. DiLeo RA, Landi BJ and Raffaelle RP. Purity assessment of multiwalled carbon nanotubes by Raman spectroscopy. *Journal of Applied Physics.* 2007; 101:0643071-0643075 http://dx.doi.org/10.1063/1.2712152